Supplementary Information (SI) for Chemical Communications.
This journal is © The Royal Society of Chemistry 2025

Supporting Information

for

Unveiled Open-Shell Nature of Antiaromatic Molecule by Surface–Molecule Interaction: A Concept Suggestion by Spin-Projected Density Functional Theory

Kohei Tada[a,b*], *Ryota Sugimori*[a], *Ryohei Kishi*[a,b,c,d], *Yasutaka Kitagawa*[a,b,c,d,e]

[a] Department of Materials Engineering Science, Graduate School of Engineering Science, The University of Osaka, Toyonaka, Osaka 560-8531, Japan

[b] Innovative Catalysis Science Division, Institute for Open and Transdisciplinary Research Initiatives (ICS-OTRI), The University of Osaka, Suita, Osaka 565-0871, Japan

[c] Center for Quantum Information and Quantum Biology (QIQB), International Advanced Research Institute (IARI), The University of Osaka, Toyonaka, Osaka 560-0043, Japan

[d] Research Center for Solar Energy Chemistry (RCSEC), Graduate School of Engineering Science, The University of Osaka, Toyonaka, Osaka 560-8531, Japan

[e] Spintronics Research Network Division, Institute for Open and Transdisciplinary Research Initiatives (OTRI-Spin), The University of Osaka, Toyonaka, Osaka 560-8531, Japan

*Corresponding Author
Phone: +81-6-6850-6267
E-mail: tada.kohei.es@osaka-u.ac.jp

Table of Contents

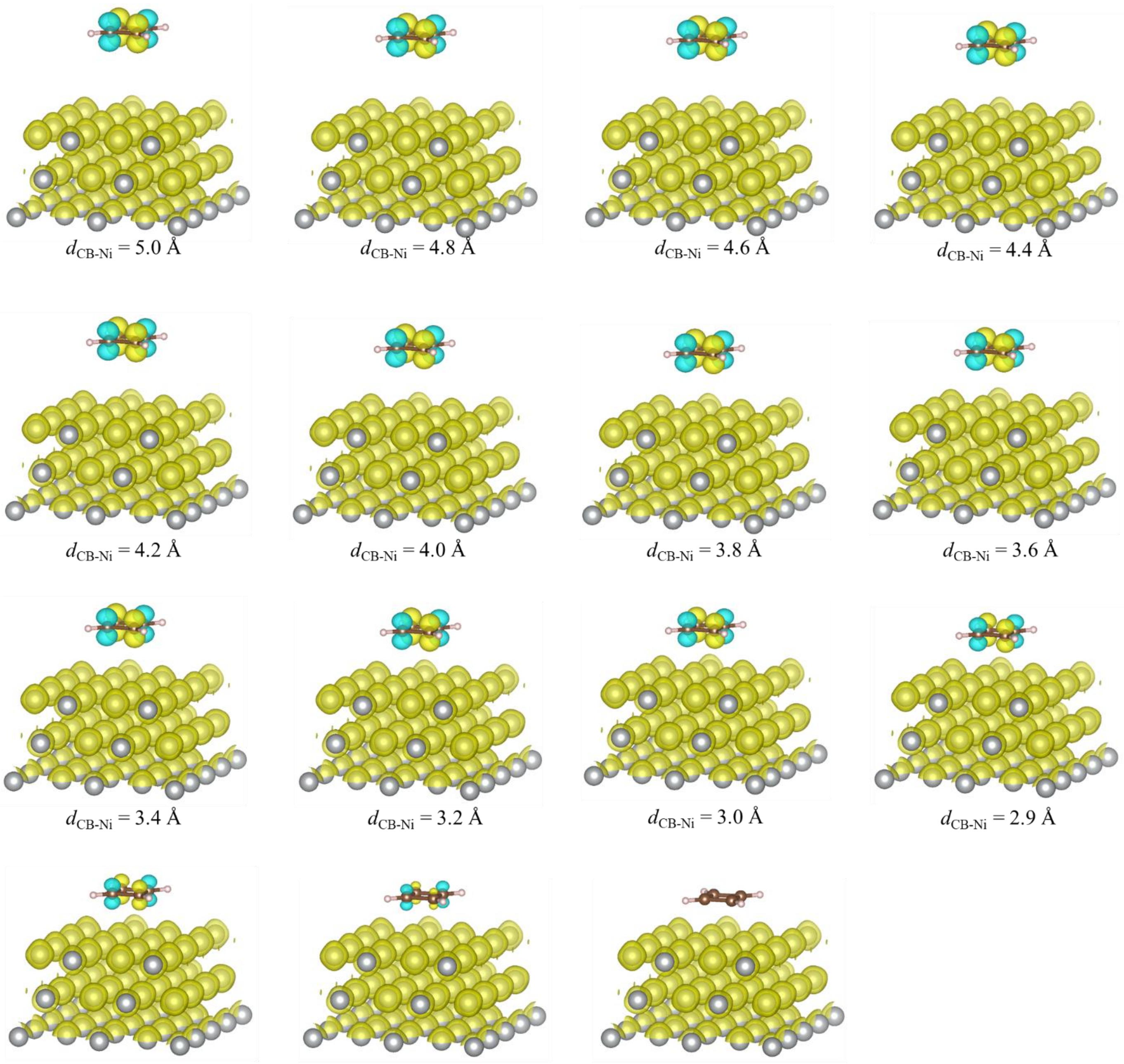

$d_{\text{CB-Ni}} = 5.0$ Å

$d_{\text{CB-Ni}} = 4.8$ Å

$d_{\text{CB-Ni}} = 4.6$ Å

$d_{\text{CB-Ni}} = 4.4$ Å

$d_{\text{CB-Ni}} = 4.2$ Å

$d_{\text{CB-Ni}} = 4.0$ Å

$d_{\text{CB-Ni}} = 3.8$ Å

$d_{\text{CB-Ni}} = 3.6$ Å

$d_{\text{CB-Ni}} = 3.4$ Å

$d_{\text{CB-Ni}} = 3.2$ Å

$d_{\text{CB-Ni}} = 3.0$ Å

$d_{\text{CB-Ni}} = 2.9$ Å

$d_{\text{CB-Ni}} = 2.8$ Å

$d_{\text{CB-Ni}} = 2.7$ Å

$d_{\text{CB-Ni}} = 2.6$ Å

Figure S1. Spin-density distributions of open-singlet states. Yellow and blue represent the distributions for alpha and beta electrons, respectively. The threshold is 0.015 e^{-}/Bohr^3. For the $d_{\text{CB-Ni}} = 2.6$ Å structure, no significant spin distribution is observed on the CB. In this structure, the electronic spins of the CB are delocalised to Ni(111), and the electronic states and energies of the $d_{\text{CB-Ni}} = 2.6$ Å structures shown in Figs. S1–S3 are difficult to distinguish at the DFT level.

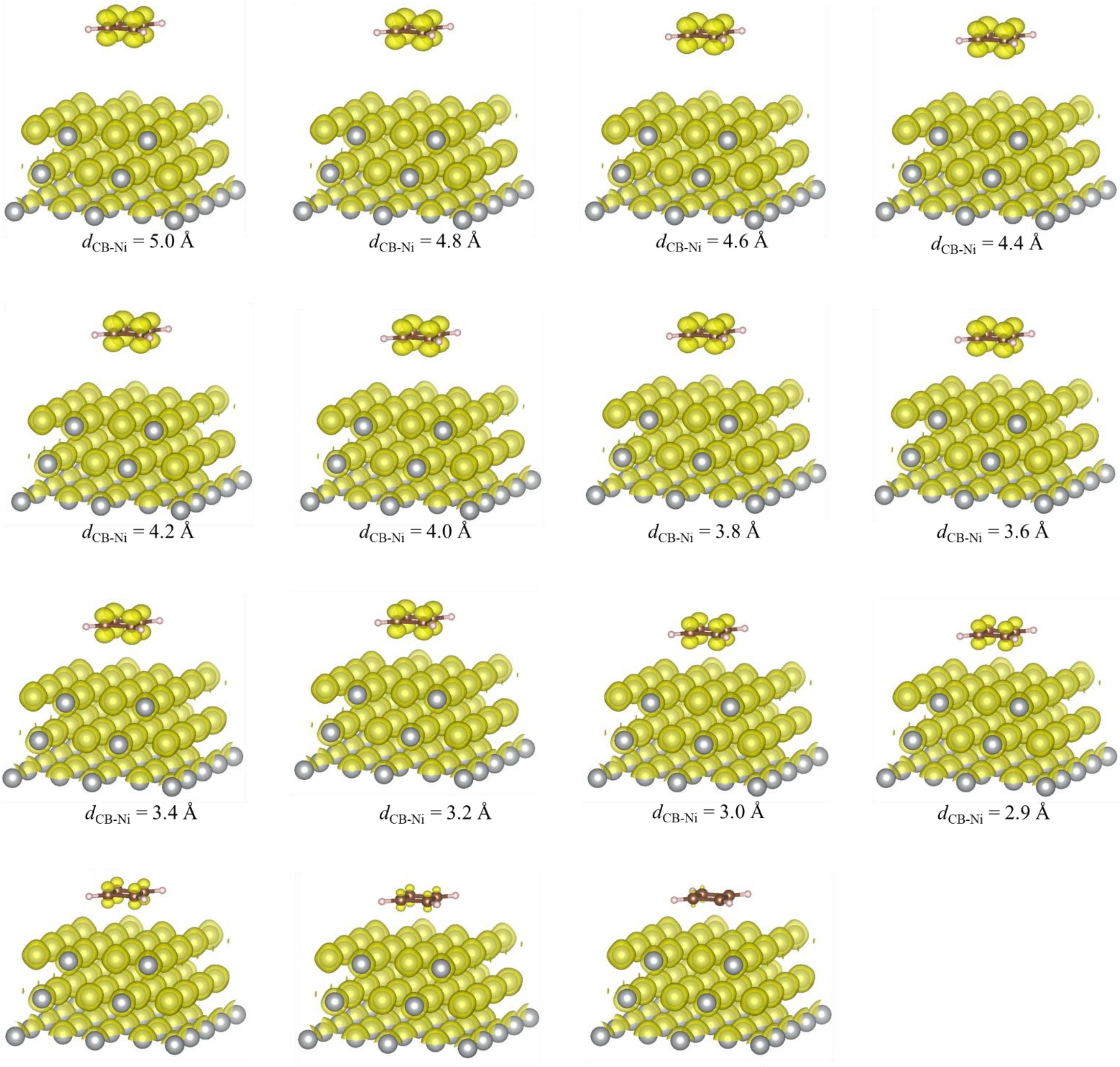

$d_{\text{CB-Ni}} = 5.0$ Å
$d_{\text{CB-Ni}} = 4.8$ Å
$d_{\text{CB-Ni}} = 4.6$ Å
$d_{\text{CB-Ni}} = 4.4$ Å
$d_{\text{CB-Ni}} = 4.2$ Å
$d_{\text{CB-Ni}} = 4.0$ Å
$d_{\text{CB-Ni}} = 3.8$ Å
$d_{\text{CB-Ni}} = 3.6$ Å
$d_{\text{CB-Ni}} = 3.4$ Å
$d_{\text{CB-Ni}} = 3.2$ Å
$d_{\text{CB-Ni}} = 3.0$ Å
$d_{\text{CB-Ni}} = 2.9$ Å
$d_{\text{CB-Ni}} = 2.8$ Å
$d_{\text{CB-Ni}} = 2.7$ Å
$d_{\text{CB-Ni}} = 2.6$ Å

Figure S2. Spin-density distributions of triplet_P states. Yellow and blue represent the distributions for alpha and beta electrons, respectively. The threshold is 0.015 e^{-}/Bohr^3. In this structure, the electronic spins of the CB are delocalised to Ni(111), and the electronic states and energies of the $d_{\text{CB-Ni}} = 2.6$ Å structures shown in Figs. S1–S3 are difficult to distinguish at the DFT level.

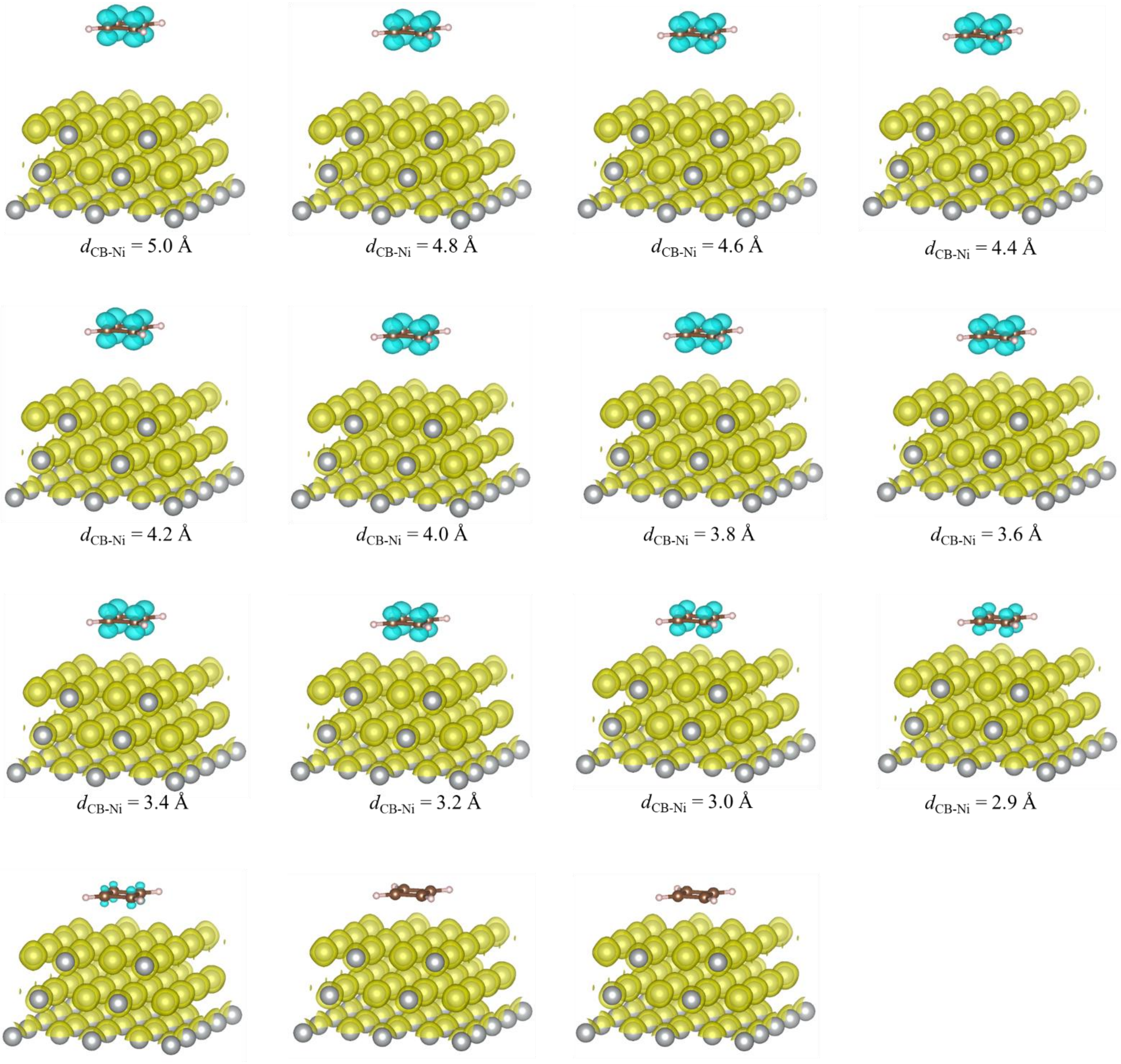

$d_{\text{CB-Ni}}$ = 5.0 Å
$d_{\text{CB-Ni}}$ = 4.8 Å
$d_{\text{CB-Ni}}$ = 4.6 Å
$d_{\text{CB-Ni}}$ = 4.4 Å
$d_{\text{CB-Ni}}$ = 4.2 Å
$d_{\text{CB-Ni}}$ = 4.0 Å
$d_{\text{CB-Ni}}$ = 3.8 Å
$d_{\text{CB-Ni}}$ = 3.6 Å
$d_{\text{CB-Ni}}$ = 3.4 Å
$d_{\text{CB-Ni}}$ = 3.2 Å
$d_{\text{CB-Ni}}$ = 3.0 Å
$d_{\text{CB-Ni}}$ = 2.9 Å
$d_{\text{CB-Ni}}$ = 2.8 Å
$d_{\text{CB-Ni}}$ = 2.7 Å
$d_{\text{CB-Ni}}$ = 2.6 Å

Figure S3. Spin-density distributions of triplet_AP states. Yellow and blue represent the distributions for alpha and beta electrons, respectively. The threshold is 0.015 e^-/Bohr^3. In this structure, the electronic spins of the CB are delocalised to Ni(111), and the electronic states and energies of the $d_{\text{CB-Ni}}$ = 2.6 Å structures shown in Figs. S1–S3 are difficult to distinguish at the DFT level. In addition, no significant spin distribution on the CB is observed at $d_{\text{CB-Ni}}$ = 2.7 Å, which is due to the effect of self-interaction error in DFT.

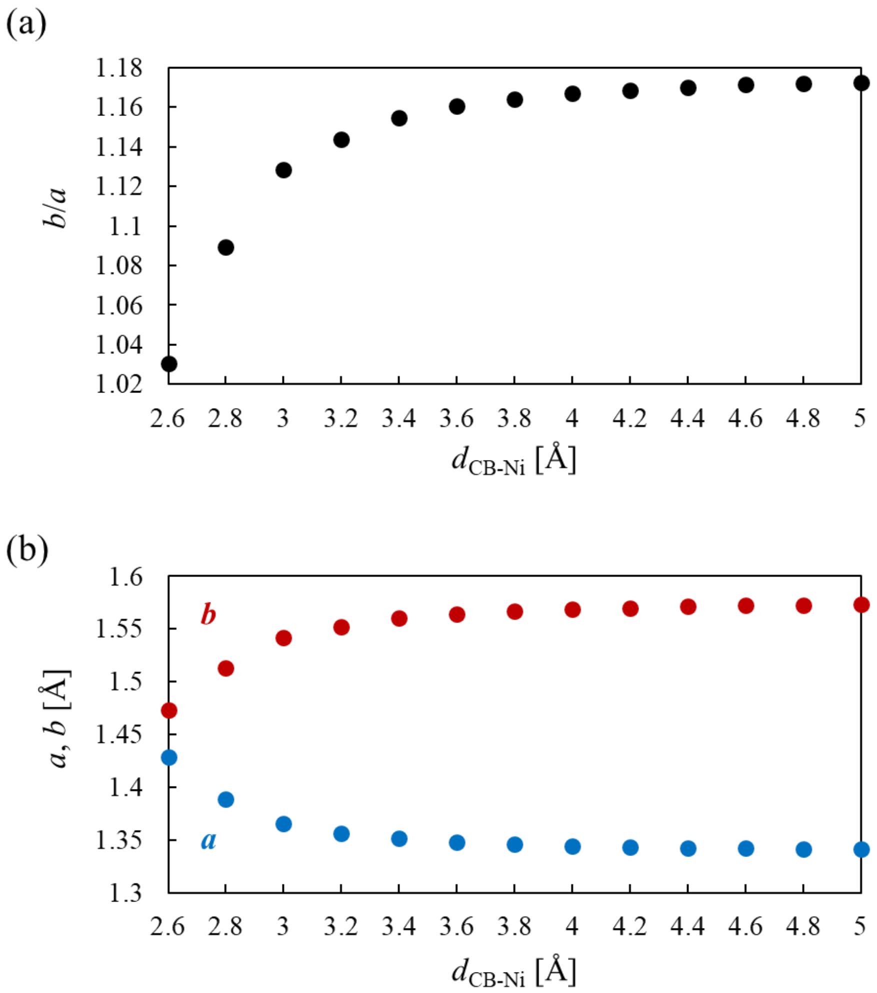

Figure S4. Variation in bond length (a: short side; b: long side) vs. $d_{\text{CB-Ni}}$ of CB/Ni(111) system with singlet state. (a) Results for a/b ratio, and (b) specific values of a and b. In this calculation, geometry optimisation was performed for both open-shell and closed-shell singlet states. In regions where the open-shell singlet state is stable, the optimisation converged to the closed-shell singlet. Therefore, the results shown in (a) and (b) are the results of a closed-shell singlet. Optimisation preserving the open-shell singlet is difficult because radicals on CB delocalise to Ni, even with slight structural changes owing to self-interaction errors. When correcting for the self-interaction error, such as on-site Coulomb correction to the π orbitals, the open-shell singlet state would be converged as a ground state with optimised D_{4h} geometry, although the search for optimal corrections is beyond the purpose of this study.

Supplementary Note:

Arrangement of spin-projection scheme of DFT/plane-wave

General Introduction for Spin Contamination and Diradical Analysis

The all-electron wave functions estimated using spin-polarised single-reference calculations for open-shell electronic states are not eigenfunctions of the total spin operator [s1, s2]. Using the spin non-polarised one-electron wavefunctions (ψ_{HOMO} and ψ_{LUMO}), the Slater determinant of the spin-polarised wavefunction, Ψ_{SP}, for the two radical electrons is written as Eq. (s1).

$$|\Psi_{\mathrm{SP}}\rangle = \frac{1}{\sqrt{2}}\begin{vmatrix} \alpha(\omega_1)\psi^{(\alpha)}_{\mathrm{SOMO}}(\mathbf{r_1}) & \beta(\omega_1)\psi^{(\beta)}_{\mathrm{SOMO}}(\mathbf{r_1}) \\ \alpha(\omega_2)\psi^{(\alpha)}_{\mathrm{SOMO}}(\mathbf{r_2}) & \beta(\omega_2)\psi^{(\beta)}_{\mathrm{SOMO}}(\mathbf{r_2}) \end{vmatrix}, \tag{s1-a}$$

$$\psi^{\alpha}_{\mathrm{SOMO}} = \cos\theta\,\psi_{\mathrm{HOMO}} + \sin\theta\,\psi_{\mathrm{LUMO}}, \tag{s1-b}$$

$$\psi^{\beta}_{\mathrm{SOMO}} = \cos\theta\,\psi_{\mathrm{HOMO}} - \sin\theta\,\psi_{\mathrm{LUMO}}, \tag{s1-c}$$

where $\alpha(\omega_x)$ and $\beta(\omega_x)$ are spin functions that correspond to up and down spins, respectively; ω_x and $\mathbf{r_x}$ are the spatial and spin coordinates of electron x, respectively; and θ is a mixing parameter of the HOMO and LUMO. The HOMO is the spin-unpolarised orbital occupied by two radical electrons in the ground-state configuration, the LUMO is the spin-unpolarised orbital occupied in the excited configuration, and the SOMO is the spin-polarised orbital occupied by only one electron, that is, the origin of magnetism. Then,

$$|\Psi_{\mathrm{SP}}\rangle = \frac{\cos^2\theta}{\sqrt{2}}\begin{vmatrix} \alpha(\omega_1)\psi_{\mathrm{HOMO}}(\mathbf{r_1}) & \beta(\omega_1)\psi_{\mathrm{HOMO}}(\mathbf{r_1}) \\ \alpha(\omega_2)\psi_{\mathrm{HOMO}}(\mathbf{r_2}) & \beta(\omega_2)\psi_{\mathrm{HOMO}}(\mathbf{r_2}) \end{vmatrix} - \frac{\sin^2\theta}{\sqrt{2}}\begin{vmatrix} \alpha(\omega_1)\psi_{\mathrm{LUMO}}(\mathbf{r_1}) & \beta(\omega_1)\psi_{\mathrm{LUMO}}(\mathbf{r_1}) \\ \alpha(\omega_2)\psi_{\mathrm{LUMO}}(\mathbf{r_2}) & \beta(\omega_2)\psi_{\mathrm{LUMO}}(\mathbf{r_2}) \end{vmatrix} - \frac{\cos\theta\sin\theta}{\sqrt{2}}\left\{\begin{vmatrix} \alpha(\omega_1)\psi_{\mathrm{HOMO}}(\mathbf{r_1}) & \beta(\omega_1)\psi_{\mathrm{LUMO}}(\mathbf{r_1}) \\ \alpha(\omega_2)\psi_{\mathrm{HOMO}}(\mathbf{r_2}) & \beta(\omega_2)\psi_{\mathrm{LUMO}}(\mathbf{r_2}) \end{vmatrix} - \begin{vmatrix} \alpha(\omega_1)\psi_{\mathrm{LUMO}}(\mathbf{r_1}) & \beta(\omega_1)\psi_{\mathrm{HOMO}}(\mathbf{r_1}) \\ \alpha(\omega_2)\psi_{\mathrm{LUMO}}(\mathbf{r_2}) & \beta(\omega_2)\psi_{\mathrm{HOMO}}(\mathbf{r_2}) \end{vmatrix}\right\}. \tag{s2}$$

Eq. (s2) is an expansion of the Slater determinant for the spin-polarised wave functions of two radical electrons, where the second term corresponds to a two-electron excitation configuration from the occupied to the unoccupied orbitals. The contribution of the two-electron excitation configuration is called the diradical character and is a characteristic quantity of diradical molecules [s3–s5]. Diradical character correlates with optical properties [s6–s8], electronic conductivity [s9], and chemical reactivity [s10, s11], which have been verified both theoretically and experimentally; hence, the diradical character has been analysed for the *in silico* design of functional open-shell molecules. More details on diradical analysis for material design can be found in some excellent review papers [s5, s6].

The first and second terms in Eq. (s2) are the singlet states, and the third term is the triplet excitation configuration. Owing to the third term, the spin-polarised wavefunction, Ψ_{SP}, is not the eigenfunction of the square of the total spin operator, $\hat{\mathrm{S}}^2$ [s1, s2]. The contamination of higher-order spin states is called the spin-contamination error (SCE) and is always included in spin-polarised wave functions by spin-polarised DFT calculations [s2]. Therefore, to estimate the diradical character from Ψ_{SP}, the SCE should be corrected, and the spin-projected diradical character proposed by Yamaguchi (hereafter, *y* value) is widely used [s3, s5] (Eq. (s3)).

$$y = 1 - \frac{2\left\langle \psi_{\mathrm{SOMO}}^{(\alpha)} \middle| \psi_{\mathrm{SOMO}}^{(\beta)} \right\rangle}{1 + \left\langle \psi_{\mathrm{SOMO}}^{(\alpha)} \middle| \psi_{\mathrm{SOMO}}^{(\beta)} \right\rangle^2} = 1 - \frac{2T}{1+T^2}. \tag{s3}$$

T in Eq. (s3) corresponds to the effective bond order between the two radical sites and is used as a chemical index for open-shell molecules, where *T* = 1 is defined as a closed-shell state, and *T* = 0 is a complete open-shell state (dominated by classical magnetic interactions). Therefore, *T* is a measure of the orbital interactions (covalent interactions) between radicals.

SCE also has an impact on the total energy. This is a particular issue in the calculation of magnetic molecules. Several correction formulae have been proposed. Three well-known formulae for magnetic coupling between two sites (a-site and b-site), J_{ab}, are

$$J_{\mathrm{ab}} = \frac{E_{\mathrm{SP}}^{\mathrm{LS}} - E_{\mathrm{SP}}^{\mathrm{HS}}}{S_{\mathrm{max}}^2} \tag{s4}$$

$$J_{\mathrm{ab}} = \frac{E_{\mathrm{SP}}^{\mathrm{LS}} - E_{\mathrm{SP}}^{\mathrm{HS}}}{S_{\mathrm{max}}(S_{\mathrm{max}}+1)} \tag{s5}$$

$$J_{\mathrm{ab}} = \frac{E_{\mathrm{SP}}^{\mathrm{LS}} - E_{\mathrm{SP}}^{\mathrm{HS}}}{\langle \hat{\mathrm{S}}^2 \rangle_{\mathrm{SP}}^{\mathrm{HS}} - \langle \hat{\mathrm{S}}^2 \rangle_{\mathrm{SP}}^{\mathrm{LS}}} \tag{s6}$$

S_{max} is the maximum total spin in the system. Eq. (s4) introduces an approximation of the classical limit proposed by Ruiz and Bencini [s12, s13]. Eq. (s5) is a formula proposed by Ginsberg, Noodleman, and Davidson that is valid in the quantum limit, that is, the region where the orbital correlation between the two sites is significantly large [s14, s15]. Eq. (s6) is called Yamaguchi's equation and bridges these two limits (classical: Eq. (s4)) and quantum (Eq. (s5)) [s16, s17]. In Eq. (s6), $\langle \hat{\mathrm{S}}^2 \rangle_{\mathrm{SP}}$ is the expectation value of the square of the total spin operator of Ψ_{SP}, and the approximation in Eq. (s7) holds when the interaction between the two sites is weak.

$$\langle \hat{\mathrm{S}}^2 \rangle_{\mathrm{SP}}^{\mathrm{HS}} \approx S_{\mathrm{max}}(S_{\mathrm{max}}+1) \tag{s7-a}$$

$$\langle \hat{\mathrm{S}}^2 \rangle_{\mathrm{SP}}^{\mathrm{LS}} \approx S_{\mathrm{max}} \tag{s7-b}$$

Substituting Eq. (s7) into Eq. (s6) yields Eq. (s4). Similarly, at the quantum limit, the approximations in Eq. (s8) hold.

$$\langle \hat{\mathrm{S}}^2 \rangle_{\mathrm{SP}}^{\mathrm{HS}} \approx S_{\mathrm{max}}(S_{\mathrm{max}}+1) \tag{s8-a}$$

$$\langle \hat{\mathrm{S}}^2 \rangle_{\mathrm{SP}}^{\mathrm{LS}} \approx 0 \tag{s8-b}$$

From Eq. (s8) and Eq. (s6), Eq. (s5), was derived. The correction of the SCE using Yamaguchi's equation is known as the approximate spin-projection (AP) method.

The AP method corrects for spin-contamination errors (SCEs) in Ψ_{SP} by projecting onto the two-site spin Heisenberg Hamiltonian (Eq. (s9)) [s16, s18]:

$$\hat{\mathrm{H}}_{\mathrm{HB}} = -2J_{\mathrm{ab}} \hat{\mathrm{s}}_{\mathrm{a}} \cdot \hat{\mathrm{s}}_{\mathrm{b}} \tag{s9}$$

The square of the total spin operator is

$$\hat{\mathrm{S}}^2 = \hat{\mathrm{s}}_{\mathrm{a}}^2 + \hat{\mathrm{s}}_{\mathrm{b}}^2 - 2\hat{\mathrm{s}}_{\mathrm{a}} \cdot \hat{\mathrm{s}}_{\mathrm{b}} \tag{s10}$$

Then, from Eq. (s9) and Eq. (s10), the expected value of $\hat{\mathrm{H}}_{\mathrm{HB}}$ can be calculated using Eq. (s11).

$$\langle \Psi | \hat{\mathrm{H}}_{\mathrm{HB}} | \Psi \rangle = -J_{\mathrm{ab}}(\langle \hat{\mathrm{S}}^2 \rangle - \langle \hat{\mathrm{s}}_{\mathrm{a}}^2 \rangle - \langle \hat{\mathrm{s}}_{\mathrm{b}}^2 \rangle) \tag{s11}$$

Assuming that the amount of spin at each site does not depend on the spin state (HS: high spin; LS: low spin), the projection of Eq. (s11) into J_{ab} yields Eq. (s12).

$$J_{\mathrm{ab}} = \frac{\left\langle \Psi_{\mathrm{SA}}^{\mathrm{LS}} \middle| \widehat{\mathrm{H}}_{\mathrm{HB}} \middle| \Psi_{\mathrm{SA}}^{\mathrm{LS}} \right\rangle - \left\langle \Psi_{\mathrm{SA}}^{\mathrm{HS}} \middle| \widehat{\mathrm{H}}_{\mathrm{HB}} \middle| \Psi_{\mathrm{SA}}^{\mathrm{HS}} \right\rangle}{\langle \hat{\mathrm{S}}^2 \rangle_{\mathrm{exact}}^{\mathrm{HS}} - \langle \hat{\mathrm{S}}^2 \rangle_{\mathrm{exact}}^{\mathrm{LS}}} = \frac{E_{\mathrm{SP}}^{\mathrm{LS}} - E_{\mathrm{SP}}^{\mathrm{HS}}}{\langle \hat{\mathrm{S}}^2 \rangle_{\mathrm{SP}}^{\mathrm{HS}} - \langle \hat{\mathrm{S}}^2 \rangle_{\mathrm{SP}}^{\mathrm{LS}}} \tag{s12}$$

$\langle \hat{\mathrm{S}}^2 \rangle_{\mathrm{exact}}$ is the exact value of $\langle \hat{\mathrm{S}}^2 \rangle$, that is, the eigenvalue of spin-adapted wave function Ψ_{SA} for $\hat{\mathrm{S}}^2$. A key point of Eq. (s12), J_{ab} can be calculated from the expected values of the total spin operators and wave functions of all electrons, which are the standard outputs of quantum chemical calculations. To obtain Eq. (s12), we assumed a two-site spin state. Hence, for multi-spin states, we cannot use $\langle \hat{\mathrm{S}}^2 \rangle$ for spin projection, and Eq. (s12).

In molecular orbital calculations, diradical and effective bond order analyses based on Eq. (s3) and energy analyses based on Eq. (s12) are generally used. However, these calculations require orbital information; specifically, T in Eq. (s3) and $\langle \hat{\mathrm{S}}^2 \rangle$ in Eq. (s12) require the overlap of the single-electron wavefunctions (orbitals). The wavefunction of surface-adsorption systems optimised by DFT/plane-wave, which is a standard first-principles approach for solid materials, requires large storage, and a transformation of the boundary conditions of the wavefunction (periodic system → isolated system) is necessary to apply these equations. The artefacts of the analysis are difficult to eliminate in this conversion, and owing to the large amount of storage required for the wavefunction file, performing analyses based on Eqs. (3) and (12) using the results calculated by the DFT/plane-wave is unrealistic.

Brief Explanation of the AP-DFT/plane-wave Scheme

The aforementioned issue of applying the AP method to DFT/plane-wave calculations can be overcome using charge densities instead of wave functions. Although the methods to estimate $\langle \hat{\mathrm{S}}^2 \rangle_{\mathrm{SP}}$ for the DFT method are still under debate [s19–s22], the results obtained from the AP scheme are almost independent of the estimation scheme of $\langle \hat{\mathrm{S}}^2 \rangle_{\mathrm{SP}}$

[s20]. By estimating $\langle \hat{S}^2 \rangle_{\mathrm{SP}}$ using the formula proposed by Wang et al. (Eq. (s13)) [s19], Eq. (s12) can be applied to the calculated DFT/plane-wave results [s23, s24].

$$\langle \hat{S}^2 \rangle_{\mathrm{SP}} = S(S+1) - \rho_{-} \tag{s13-a}$$

$$S = \frac{1}{2}\left(\int \rho^{(\alpha)}(r)dr - \int \rho^{(\beta)}(r)dr\right) \tag{s13-b}$$

$$\rho_{-} = \int \rho_{-}(r)dr \tag{s13-c}$$

$$\rho_{-}(r) = \begin{cases} \rho_{\alpha}(r) - \rho_{\beta}(r) & when\ \rho^{(\alpha)}(r) - \rho^{(\beta)}(r) < 0 \\ 0 & when\ \rho^{(\alpha)}(r) - \rho^{(\beta)}(r) \geq 0 \end{cases} \tag{s13-d}$$

The $\langle \hat{S}^2 \rangle_{\mathrm{SP}}$ values of DFT are often calculated using Eq. (s14), which is derived for Hartree–Fock method [s1].

$$\langle \hat{S}^2 \rangle_{\mathrm{SP}} = \langle \hat{S}^2 \rangle_{\mathrm{exact}} + N_{\beta} - \textstyle\sum_{i,j}^{occ.} \left\langle \psi_i^{(\alpha)} \middle| \psi_j^{(\beta)} \right\rangle^2 \tag{s14}$$

According to Wang et al., Eq. (s14) is the non-interaction limit of the DFT [s19]. The difference between the values obtained using Eqs. (s13) and (s14) are determined to be C$_{\mathrm{int}}$, and by simultaneously solving the equations of $\langle \hat{S}^2 \rangle_{\mathrm{SP}}$ for the LS and HS states, we obtain Eq. (s15) [s25].

$$T^2 = 1 + \rho_{-}^{\mathrm{LS}} + S^{\mathrm{HS}}\left(S^{\mathrm{HS}} + 1\right) - \rho_{-}^{\mathrm{HS}} - \langle \hat{S}^2 \rangle_{\mathrm{exact}}^{\mathrm{HS}} - \textstyle\sum_{i,\mathrm{excluding\ SOMO}}^{occ.} \left(\left\langle \psi_i^{\mathrm{LS}(\alpha)} \middle| \psi_i^{\mathrm{LS}(\beta)} \right\rangle^2 - \left\langle \psi_i^{\mathrm{HS}(\alpha)} \middle| \psi_i^{\mathrm{HS}(\beta)} \right\rangle^2 \right) - \textstyle\sum_{i \neq j}^{occ.} \left(\left\langle \psi_i^{\mathrm{LS}(\alpha)} \middle| \psi_j^{\mathrm{LS}(\beta)} \right\rangle^2 - \left\langle \psi_i^{\mathrm{HS}(\alpha)} \middle| \psi_j^{\mathrm{HS}(\beta)} \right\rangle^2 \right) + \left(\mathrm{C}_{\mathrm{int}}^{\mathrm{LS}} - \mathrm{C}_{\mathrm{int}}^{\mathrm{HS}}\right) \tag{s15}$$

To estimate the *T* value using only the electron-density distribution, we applied the following approximation [s25]:

$$\left\langle \psi_{i \neq \mathrm{SOMO}}^{\mathrm{LS}(\alpha)} \middle| \psi_{i \neq \mathrm{SOMO}}^{\mathrm{LS}(\beta)} \right\rangle^2 \approx \left\langle \psi_{i \neq \mathrm{SOMO}}^{\mathrm{HS}(\alpha)} \middle| \psi_{i \neq \mathrm{SOMO}}^{\mathrm{HS}(\beta)} \right\rangle^2 \tag{s16}$$

$$\left\langle \psi_i^{\mathrm{LS}(\alpha)} \middle| \psi_j^{\mathrm{LS}(\beta)} \right\rangle^2 \approx \left\langle \psi_i^{\mathrm{HS}(\alpha)} \middle| \psi_j^{\mathrm{HS}(\beta)} \right\rangle^2 \tag{s17}$$

$$\mathrm{C}_{\mathrm{int}}^{\mathrm{LS}} \approx \mathrm{C}_{\mathrm{int}}^{\mathrm{HS}} \tag{s18}$$

We then obtained the formula for *y* values by electron density (Eq. (s19)) [s25, s26].

$$y = 1 - \frac{2\sqrt{1 + \rho_{-}^{\mathrm{LS}} - \rho_{-}^{\mathrm{HS}}}}{2 + \rho_{-}^{\mathrm{LS}} - \rho_{-}^{\mathrm{HS}}}. \tag{s19}$$

Here, the *T* value, which is the effective intra-radical bond order, is

$$T = \sqrt{1 + \rho_{-}^{\mathrm{LS}} - \rho_{-}^{\mathrm{HS}}} \quad \text{(s20)}$$

The approximate accuracy of Eq. (s19) and Eq. (s20) was verified using the hybrid DFT method and found to be in good agreement with the values obtained from Eq. (s3) [s25]. Furthermore, we compared this method with a multi-reference method [s27]. The diradical character can be determined directly by performing calculations above the CISD level. A comparison of the results of the AP-DFT/plane-wave method and CASSCF calculations using the metal dimer models confirmed qualitative agreement, although the influence of the self-interaction error still remains [s27].

Combination with General Spin-Projection Scheme

Using Eq. (s13), Eq. (s19), and Eq. (s20), we can analyse the SCE, diradical character, and effective bond order from the results calculated using spin-polarised DFT/plane-wave. However, these equations are tabular for two-site spin systems. This is a constraint owing to the AP method: projection onto the two-site Heisenberg Hamiltonian. This constraint allows for a series of derivations using $\langle \hat{\mathrm{S}}^2 \rangle_{\mathrm{SP}}$. The CB/Ni(111) system investigated in this study is a multi-spin system; therefore, it is necessary to remove this constraint. The spin correlation function, $\langle \hat{\mathrm{s}}_{\mathrm{a}} \cdot \hat{\mathrm{s}}_{\mathrm{b}} \rangle$, solves this multi-spin-state issue [s28–s30].

$$\langle \Psi | \hat{\mathrm{H}}_{\mathrm{HB}} | \Psi \rangle = -2J_{\mathrm{ab}} \langle \hat{\mathrm{s}}_{\mathrm{a}} \cdot \hat{\mathrm{s}}_{\mathrm{b}} \rangle. \quad \text{(s21)}$$

Eq. (s21), a formula for two-spin systems, can easily be extended to multi-spin systems (Eq. (s22)).

$$\langle \Psi | \hat{\mathrm{H}}_{\mathrm{HB}} | \Psi \rangle = -2 \textstyle\sum_{\mathrm{i} > \mathrm{j}} J_{\mathrm{ij}} \langle \hat{\mathrm{s}}_{\mathrm{i}} \cdot \hat{\mathrm{s}}_{\mathrm{j}} \rangle. \quad \text{(s22)}$$

$\hat{\mathrm{s}}_{\mathrm{i}}$ is a spin operator for spin site i. Although the estimation scheme of the spin-correlation function based on the results of the DFT calculations is still under debate, in this study, we used the formula in the generalised spin projection proposed by Shoji et al. [s28]:

$$\langle \hat{\mathrm{s}}_{\mathrm{i}} \cdot \hat{\mathrm{s}}_{\mathrm{j}} \rangle^{\mathrm{HS}} = |\hat{\mathrm{s}}_{\mathrm{i}}| \cdot |\hat{\mathrm{s}}_{\mathrm{i}}| \quad \text{(s23)}$$

$$\langle \hat{\mathrm{s}}_{\mathrm{i}} \cdot \hat{\mathrm{s}}_{\mathrm{j}} \rangle^{\mathrm{LS}} = -|\hat{\mathrm{s}}_{\mathrm{i}}| \cdot |\hat{\mathrm{s}}_{\mathrm{i}}| - \frac{\mathrm{N}_{\beta}}{2} {T_{\mathrm{ij}}}^{2} \tag{s24}$$

${T_{\mathrm{ij}}}^2$ is the square of the effective bond order between sites i and j, and N_{β} is the number of β electrons. When ${T_{\mathrm{ij}}}^2$, N_{β}, and the total energy are obtained, Eq. (s22)–(s24) yield the J_{ij} values.

The three open-shell electronic states investigated in this study were approximated as four spin sites within the classical limit (Fig. S5), and quantum effects were incorporated into Eq. (s24), owing to orbital correlations. In Fig. S5, sites a and b are the spin sites in the CB, and sites c and d are the spin sites on the Ni (111) surface with which the CB interacts. The wavefunctions ϕ_1 (Fig. S5(a)), ϕ_2 (Fig. S5(b)), and ϕ_3 (Fig. S5(c)) correspond to the triplet_P (Fig. 2(d)), open singlet (Fig. 2(c)), and triplet_AP (Fig. 2(e)) electronic states. J_1, J_2, and J_3 are the J_{ij} values of (i, j) = (a, b), (a, c), and (c, d), respectively; in other words, these J values are the magnetic coupling in CB, between CB and the Ni surface, and on the Ni surface. Similarly, T_1 and T_2 are the effective bond orders between a and b, and between a and c, respectively. Then, Eq. (s25)–(s27) are obtained from Eq. (s22)–(s24).

$$E_1 \equiv \langle \phi_1 | \hat{\mathrm{H}}_{\mathrm{HB}} | \phi_1 \rangle = -2J_1 |\hat{\mathrm{s}}_{\mathrm{a}}| \cdot |\hat{\mathrm{s}}_{\mathrm{b}}| - 4J_2 |\hat{\mathrm{s}}_{\mathrm{a}}| \cdot |\hat{\mathrm{s}}_{\mathrm{c}}| - 2J_3 |\hat{\mathrm{s}}_{\mathrm{c}}| \cdot |\hat{\mathrm{s}}_{\mathrm{d}}|, \tag{s25}$$

$$E_2 \equiv \langle \phi_2 | \hat{\mathrm{H}}_{\mathrm{HB}} | \phi_2 \rangle = -2J_1 \left(-|\hat{\mathrm{s}}_{\mathrm{a}}| \cdot |\hat{\mathrm{s}}_{\mathrm{b}}| - \frac{{T_1}^2}{2} \right) - 2J_2 |\hat{\mathrm{s}}_{\mathrm{a}}| \cdot |\hat{\mathrm{s}}_{\mathrm{c}}| - 2J_2 \left(-|\hat{\mathrm{s}}_{\mathrm{a}}| \cdot |\hat{\mathrm{s}}_{\mathrm{c}}| - \frac{{T_2}^2}{2} \right) - 2J_3 |\hat{\mathrm{s}}_{\mathrm{c}}| \cdot |\hat{\mathrm{s}}_{\mathrm{d}}| \quad , \tag{s26}$$

$$E_3 \equiv \langle \phi_3 | \hat{\mathrm{H}}_{\mathrm{HB}} | \phi_3 \rangle = -2J_1 |\hat{\mathrm{s}}_{\mathrm{a}}| \cdot |\hat{\mathrm{s}}_{\mathrm{b}}| - 4J_2 \left(-|\hat{\mathrm{s}}_{\mathrm{a}}| \cdot |\hat{\mathrm{s}}_{\mathrm{c}}| - \frac{{T_2}^2}{2} \right) - 2J_3 |\hat{\mathrm{s}}_{\mathrm{c}}| \cdot |\hat{\mathrm{s}}_{\mathrm{d}}|. \tag{s27}$$

From Eq. (s25) and Eq. (s27),

$$J_2 = -\frac{E_3 - E_1}{4\left(-2|\hat{\mathrm{s}}_{\mathrm{a}}| \cdot |\hat{\mathrm{s}}_{\mathrm{b}}| - \frac{{T_2}^2}{2} \right)}. \tag{s28}$$

From Eq. (s25) and Eq. (s26),

$$J_1 = -1 \times \left(\left(\frac{4|\hat{\mathrm{s}}_{\mathrm{a}}| \cdot |\hat{\mathrm{s}}_{\mathrm{c}}| + {T_2}^2}{4|\hat{\mathrm{s}}_{\mathrm{a}}| \cdot |\hat{\mathrm{s}}_{\mathrm{b}}| + {T_1}^2} \right) J_2 - \frac{E_2 - E_1}{4|\hat{\mathrm{s}}_{\mathrm{a}}| \cdot |\hat{\mathrm{s}}_{\mathrm{b}}| + {T_1}^2} \right). \tag{s29}$$

When the J values are projected, E_1, E_2, E_3, T_1, and T_2 correspond to the total energy of the triplet_P state, total energy of the open-singlet state, total energy of the triplet_AP state, ΔT in Fig. 4, and $T_{\text{triplet\_AP}}$ in Fig. 4, respectively. $|\hat{s}_a| = |\hat{s}_b| = 1/2$, where $|\hat{s}_c|$ is approximately half the value of the local magnetic moment per Ni atom.

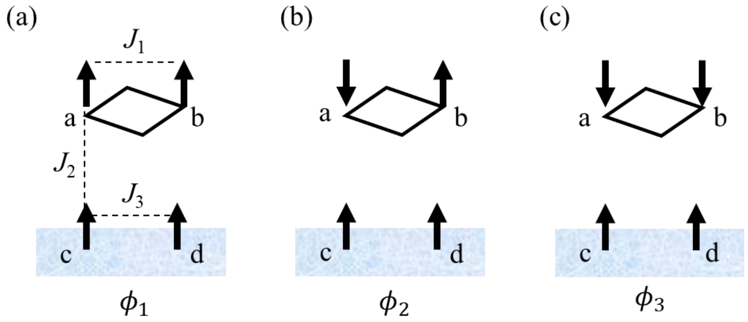

Figure S5. Spin configuration and effective magnetic exchange integrals of (a) triplet_P, (b) open-singlet, and (c) triplet_AP states of CB/Ni(111) system.

An estimation scheme for T based on the electron density was introduced in the previous section (Eq. (s20)). However, in the present study, the spin polarisation of Ni metal resulted in a negative root sign in Eq. (s20). Therefore, T values were calculated using two methods of approximation: (1) T': considering $d_{\text{CB-Ni}} = 5.0$ Å as the dissociation limit, the T value at this limit is 0; and (2) T'': considering $d_{\text{CB-Ni}} = 2.6$ Å as the quantum limit, the T value at this limit is 1. Figure S6(a) shows the results of $T_{\text{open-singlet}}$ (LS: open-singlet; HS: Triplet_P); the results for T' and T'' are in qualitative agreement, except for the convergence behaviour to the classical limit. The diradical character estimated using $T'_{\text{open-singlet}}$ and $T''_{\text{open-singlet}}$ ($y'_{\text{open-singlet}}$ and $y''_{\text{open-singlet}}$, respectively) and $y_{\text{open-singlet}}$ (when the value of the root in Eq. (s14) is negative, and the values approximating 1) are compared in Fig. S6(b). All y values decreased as the molecule–surface distance decreased, although the convergence behaviour to the dissociation limit differed.

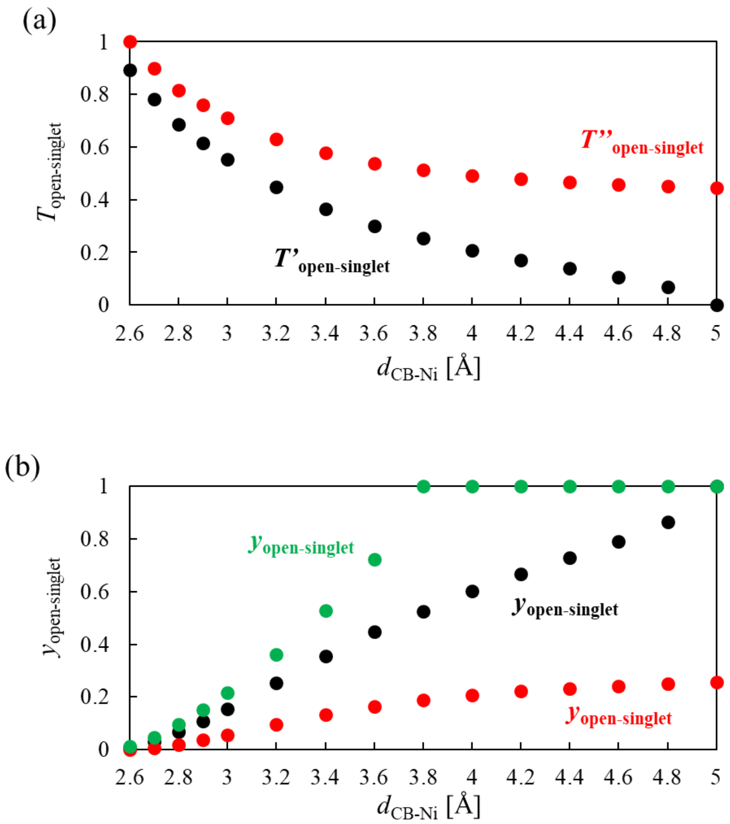

Figure S6. (a) Comparison of $T_{\text{open-singlet}}$ estimated using different definitions. (b) Comparison of $y_{\text{open-singlet}}$ estimated using different definitions.

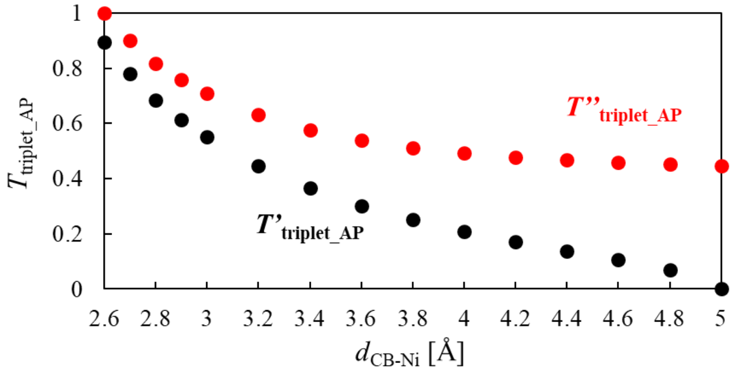

Figure S7. Comparison of $T_{\text{triplet\_AP}}$ estimated using different definitions.

A comparison of T' and T'' in triplet_AP ($T_{\text{triplet\_AP}}$) is shown in Fig. S7, where LS is triplet_AP and HS is triplet_P. Similar to $T_{\text{open-singlet}}$, a difference was observed only at the dissociation limit. Using the $T_{\text{triplet\_AP}}$ and $T_{\text{open-singlet}}$

values, diradical coupling within CB can be discussed (Fig. 4(c)), that is, the effective bond order of the diradical is approximated to the ΔT values (Eq. (s30)).

$$\Delta T = T_{\mathrm{open-singlet}} - T_{\mathrm{triplet\_AP}} \tag{s30}$$

In the triplet_AP state, T was overestimated if the maximum number of bond orders between the cyclobutadiene and Ni atoms was 1. The local magnetic moment per Ni atom is <1, and the number of electrons that can be used for the covalent bond will be <1. Therefore, we also estimated the $T_{\mathrm{triplet\_AP}}$ values with a scaling factor equal to the local magnetic moment per Ni atom (specifically, 0.7) and compared the results with and without scaling. Figure S8(a) shows the unscaled results, and Figure S8(b) presents the scaled results. Without scaling, some ΔT values are negative, and physical interpretation is difficult because T is a bond order (Fig. S8(a)). By contrast, with weighting, ΔT remains in its defined range (0 to 1) (Fig. S8(b)). Both ΔT results are consistent with the discussion in the main text, which states that $d_{\mathrm{CB\text{-}Ni}}$ decreases for $d_{\mathrm{CB\text{-}Ni}} < 3.0$ Å and reaches an extreme value at $d_{\mathrm{CB\text{-}Ni}} = 2.8$ Å. To satisfy the definition range, we used the value of $\Delta T'$ given in Fig. S4(b) to estimate J_1 using Eq. (s13); the results are shown in Fig. 4 in the main text. The method for obtaining T_{ij} for general spin projection remains an issue to be addressed. Nevertheless, the analysis in this study qualitatively shows how surface interactions affect diradical coupling.

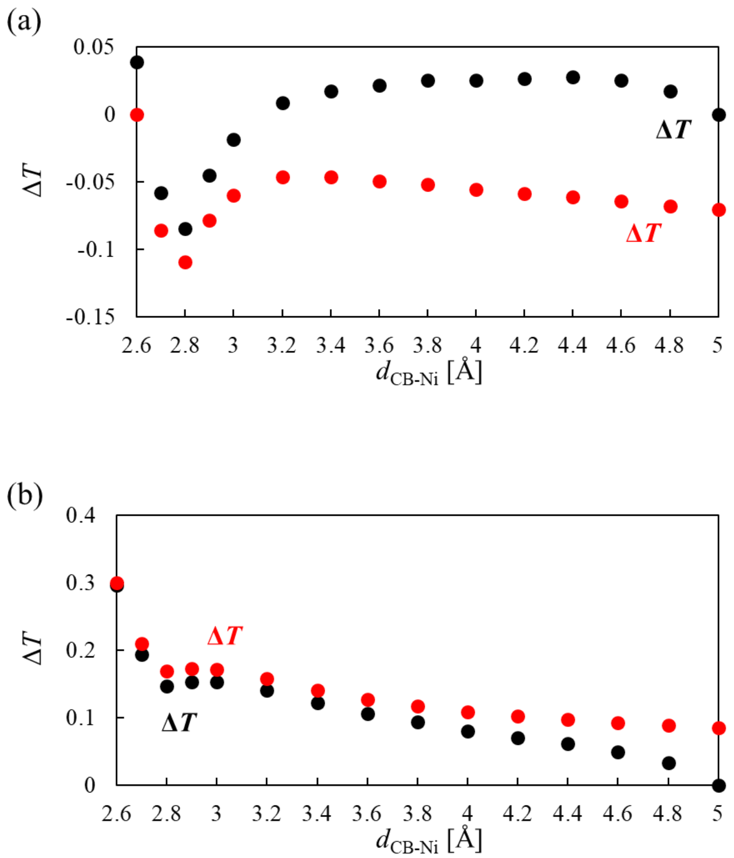

Figure S8. Comparison of $\Delta T_{\mathrm{triplet\_AP}}$ estimated using different definitions: (a) without and (b) with scaling by Ni magnetic moment. The black and red dots represent the results estimated using the T' and T'' values, respectively.

The Ni spins that should not be considered in the Heisenberg model were calculated and compared by projection onto the Heisenberg Hamiltonian. Therefore, the "correct" result for ΔT shown in Fig. S7 lies between those shown in Fig. S8(a) and Fig. S8(b). Furthermore, the SCE was not completely removed from the J values owing to these approximations. However, the tendency for the J value to decrease with surface–molecule distance is clear, and the ability to control the electronic structure of antiaromatic molecules by surfaces, which is the most important concept of this study, is retained.

Computational Method

The GGA-PBE formula [s31] was used for the exchange-correlation functional of the DFT. A plane wave was used for the basis functions, and the core region was treated using the projector-augmented wavefunction approach [s32, s33]. The electron numbers in the valence regions were set to Ni(10), C(4), and H(1). The cutoff energies were 600 eV for the wave function and 2400 eV for the augmented charge. Spin-polarised DFT/plane-wave calculations were performed using the VASP program [s34–s37], and spin projection was performed using a handmade program.

Supplementary Note References

[s1] A. Szabo and N. S. Ostlund, *Modern Quantum Chemistry: Introduction to Advanced Electronic Structure Theory* (Dover Publications, New York, 1996).

[s2] J. Kohanoff, *Electronic Structure Calculations for Solids and Molecules Theory and Computational Methods* (Cambridge University Press, Cambridge, 2006).

[s3] K. Yamaguchi, *Chem. Phys. Lett.*, 1975, **33**, 330.

[s4] K. Yamaguchi, T. Kawakami, Y. Takano, Y. Kitagawa, Y. Yamashita, and H. Fujita, *Int. J. Quantum Chem.*, 2002, **90**, 370.

[s5] T. Stuyver, B. Chen, T. Zeng, P. Geerlings, F. De Proft, and R. Hoffinann, *Chem. Rev.*, 2019, **119**, 11291.

[s6] M. Nakano, and B. Champagne, *J. Phys. Chem. Lett.*, 2015, **6**, 3236.

[s7] K. Kamada, K. Ohta, A. Shimizu, T. Kubo, R. Kishi, H. Takahashi, E. Botek, B. Champagne, and M. Nakano, *J. Phys. Chem. Lett.*, 2010, **1**, 937.

[s8] S. Muhammad, M. Nakano, A.G. Al-Sehemi, Y. Kitagawa, A. Irfan, A.R. Chaudhry, R. Kishi, S. Ito, K. Yoneda, and K. Fukuda, *Nanoscale*, 2016, **8**, 17998.

[s9] T. Stuyver, T. Zeng, Y. Tsuji, P. Geerlings and F. de Proft, *Nano Lett.*, 2018, **18**, 7298.

[s10] M. Nishijima, K. Mutoh, and J. Abe, *Chem. Lett.*, 2021, **50**, 1423.

[s11] K. Tada, H. Ozaki, K. Fujimaru, Y. Kitagawa, T. Kawakami, and M.Okumura, *Phys. Chem. Chem. Phys.*, 2021, **23**, 25024.

[s12] E. Bencini, F. Totti, C.A. Doul, K. Doclo, P. Fantucci, and V. Barone, *Inorg. Chem.*, 1997, **36**, 5022.

[s13] E. Ruiz, J. Cano, S. Alvarez, and P. Alemany, *J. Comput. Chem.*, 1999, **20**, 1391.

[s14] A.P. Ginsberg, *J. Am. Chem. Soc.*, 1986, **102**, 111.

[s15] L. Noodleman, and E.R. Davidson, *Chem. Phys.*, 1986, **109**, 131.

[s16] K. Yamaguchi, H. Fukui, and T. Fueno, *Chem. Lett.*, 1986, **15**, 625.

[s17] S. Paul, and A. Misra, *J. Chem. Theory Comput.,* 2012, **8**, 843.

[s18] K. Yamaguchi, F. Jensen, A. Dorigo, and K.N. Houk, *Chem. Phys. Lett.*, 1988, **149**, 537.

[s19] J. Wang, A.D. Becke, and V.H. Smith, *J. Chem. Phys.*, 1995, **102**, 3477.

[s20] T. Saito, S. Nishihara, S. Yamanaka, Y. Kitagawa, T. Kawakami, S. Yamada, H. Isobe, M. Okumura, and K. Yamaguchi, *Theor. Chem. Acc.*, 2011, **130**, 749.

[s21] A.J. Cohen, D.J. Tozer, and N.C. Handy, *J. Chem. Phys.*, 2007, **126**, 214104.

[s22] A.S. Menon, and L. Radom, *J. Phys. Chem. A*, 2008, **112**, 13225.

[s23] K. Tada, H. Koga, M. Okumura, and S. Tanaka, *Chem. Phys. Lett.*, 2018, **701**, 103.

[s24] K. Tada, S. Tanaka, T. Kawakami, Y. Kitagawa, M. Okumura, and K. Yamaguchi, *Appl. Phys. Express*, 2019, **12**, 115506.

[s25] K. Tada, Y. Kitagawa, T. Kawakami, M. Okumura, and S. Tanaka, *Chem. Lett.*, 2021, **50**, 392.

[s26] K. Tada, H. Ozaki, K. Fujimaru, Y. Kitagawa, T. Kawakami, and M. Okumura, *Phys. Chem. Chem. Phys.,* 2021, **23**, 25024.

[s27] K. Tada, K. Masuda, R. Kishi, and Y. Kitagawa, *Chemistry*, 2024, **6**, 1572.

[s28] M. Shoji, K. Koizumi, Y. Kitagawa, T. Kawakami, S. Yamanaka, M. Okumura, and K. Yamaguchi, *Chem. Phys. Lett.*, 2006, **432**, 343.

[s29] S. Yamanaka, R. Takeda, M. Shoji, Y. Kitagawa, H. Honda, and K. Yamaguchi, *Int. J. Quant. Chem.*, 2005, **105**, 605.

[s30] K. Tada, S. Yamanaka, T. Kawakami, Y. Kitagawa, M. Okumura, K. Yamaguchi, and S. Tanaka, *Chem. Phys. Lett.*, 2020, **765**, 138291.

[s31] J.P. Perdew, K. Burke, and M. Ernzerhof, *Phys. Rev. Lett.*, 1996, **77**, 3865.

[s32] P.E. Blöchl, *Phys. Rev. B*, 1994, **50**, 17953.

[s33] G. Kresse, and D. Joubert, *Phys. Rev. B*, 1999, **59**, 1758.

[s34] G. Kresse, and J. Hafner, *Phys. Rev. B*, 1993, **47**, 558.

[s35] G. Kresse, and J. Hafner, *Phys. Rev. B*, 1994, **49**, 14251.

[s36] G. Kresse, J. Furthmuller, *Phys. Rev. B*, 1996, **54**, 11169.

[s37] G. Kresse, and J. Furthmuller, *Comp. Mater. Sci.*, 1996, **6**, 15.